

Dark Superabsorbers with Dirac-delta-like superdirective radiation

Jeng Yi Lee

Department of Opto-Electronic Engineering, National Dong Hwa University, Hualien 974301, Taiwan

Irving Rondón

School of Computational Sciences, Korea Institute for Advanced Study, Seoul 0245, Republic Of Korea

Andrey E. Miroshnichenko

School of Engineering and Information Technology, University of New South Wales, Canberra, Australian Capital Territory 2600, Australia

Pai-Yen Chen

Department of Electrical and Computer Engineering, University of Illinois at Chicago, Illinois 60661, USA

(Dated: July 2, 2024)

We theoretically and numerically reveal that under a given level of extinction cross section and with definite angular momentum channels dominant, there exists a physical limitation for absorption cross section being maximum and scattering cross section being minimum. In addition, any scattering systems operated at this condition would be accompanied by a needle Dirac-delta-like far-field radiation pattern, reducing to perturb the background field except in the forward direction. We therefore refer to this outcome as dark superabsorbers. Moreover, by considering the mathematical Gibbs phenomenon, we find that a completely equivalent Dirac-delta far-field radiation is excluded even we could properly design the scatterers operated at such conditions. We believe this finding has potential applications in design of dark energy harvesting, lower-visibility receivers, superdirective light-matter interaction, and Fresnel diffractive imaging.

Enhancing light harvesting for any scattering systems is closely related to practical application in photovoltaics engineering, photodetectors, photothermal therapy to name a few [1–8]. However, scattering of any objects with deep subwavelength scale would suffer from single mode limit, that can be overcome by employing multi-layered structures to induce multipolar resonant modes with spectrally overlapped [9–12]. The mechanism is similar to raise degenerate surface wave modes, that can be closely related to the whispering gallery condition, as already demonstrated in superscattering [13–16]. In addition, another different mechanism to have superscattering events can get help from constructive interference between one radiation channel at bound state in the continuum and another channel at resonance [17]. We note that with a consideration of energy conservation, there has an ultimate bound on partial absorption cross section (ABS) at each scattering channel [18–20]. On the other hand, we notice that enhancing ABS would pay the price on the accumulation of extinction cross section (EXT). EXT is related to fundamental optical theorem, that can measure the amount of forward scattering amplitude in parallel with the incident wave [21, 22]. One example to discuss the relation of EXT and forward scattering amplitude is the Kerker effect, in which combining π - or 0-phase shift for electric and magnetic dipolars with equal strength would lead to have optimized backward or forward scattering, respectively [22–30]. On the other hand, based on Lorentz reciprocity, any scattering objects made of reciprocal materials would preserve EXT at two opposite illuminating directions [31]. Nevertheless such reci-

procity can be broken by exploiting optically nonlinear materials [32].

In this work, we would indicate that under a constant level of EXT, there could have a strategy to design the scatterers with not only ABS enhanced as well as scattering cross section (SCS) reduced, but also an unusual Dirac-delta-like far-field radiation. We referred to the outcome as dark superabsorbers. Our scheme is firstly by means of normalized cross section diagram, stemming from optimizing an energy function involving SCS and ABS, as shown in Fig. 1 (b) [20]. Accordingly, we can indicate generic power distribution for ABS, SCS, and EXT for any scattering systems, irrespective of system parameters. Next, with a consideration of a constant level of EXT and definite angular momentum channels dominant, we can point out the maximum ABS and the minimum SCS. Interestingly, at this condition, we find that the description of the far-field radiation pattern is mathematically equivalent to a discrete Fourier series of the Dirac-delta function. Moreover, the corresponding null-to-null bandwidth of the main lobe would be gradually reduced by more angular momentum channels properly excited, resulting in perturbing the background field except in the forward direction. However, by considering the Gibbs phenomenon of Fourier theory, the ideal (perfect) Dirac-delta radiation is excluded. Instead, it would have many ripple-like sidelobes around the main lobe. We also numerically find that the ratio of the total radiation power of these sidelobes over that of the main lobe approaches a constant as more angular momentum channels are properly excited. We believe our finding

would benefit possible applications on dark energy harvesting, lower-visibility receivers, directive light-matter interaction, and Fresnel diffractive imaging.

We consider a cylindrical scatterer illuminated by a normal incidence of an electromagnetic plane wave with linear polarization. Below, we discuss the \mathbf{p} -polarized excitation, in which the exciting magnetic field oscillates only along the z -direction, as shown in an inset of Fig. 1 (b). The formulas of ABS and SCS for arbitrary cylindrical scatterers are $\sigma_{abs} = \sum_{n=-N}^N \sigma_{abs,n} = -4/k_0 \sum_{n=-N}^N [Re[a_n] + |a_n|^2]$ and $\sigma_{scs} = \sum_{n=-N}^N \sigma_{scs,n} = 4/k_0 \sum_{n=-N}^N |a_n|^2$, respectively [33, 34]. Here $\sigma_{abs,n}$ and $\sigma_{scs,n}$ are the partial ABS and SCS, a_n is complex scattering coefficient for n -th angular momentum channel, k_0 is background wavenumber defined by $k_0 = 2\pi/\lambda_0$, and λ_0 is operating wavelength. We mark that the notation of N refers to the terminate term of the dominant cylindrical wave scattering, while $n = 0, 1, 2, \dots$ corresponds to magnetic dipole, electric dipole, and electric quadrupole, respectively. On the other hand, EXT is the summation of ABS and SCS, i.e., $\sigma_{ext} = \sigma_{abs} + \sigma_{scs}$, also linking the relation of forward scattering amplitudes [21, 22]. Thus, any passive scatterers with non-zeros ABS and SCS would accumulate EXT, causing a shadow. Moreover, due to the cylindrical symmetry at normal incidence, there has a degeneracy for $a_n = a_{-n}$.

As generic scattering systems made of passive materials embedded, from energy conservation, it ensures partial ABS subject to $\sigma_{abs,n} \geq 0$. Consequently, we can obtain a phasor condition for complex scattering coefficients established at each angular momentum channels, i.e., $|a_n| \leq 1$ and $Arg[a_n] \in [0, 2\pi)$ [19, 20]. Accordingly, we can point out the maximum partial ABS for each angular momentum channels operated at $a_n = 1/2$ and $Arg[a_n] = \pi$, corresponding to the eigenvalue zero of the scattering matrix, i.e., the coherent perfect absorption condition [35? -37]. In addition, we also find the condition of the maximum partial SCS, when the scattering systems are operated at $a_n = 1$ and $Arg[a_n] = \pi$.

The comprehension of power distribution and its physical limitation for any scattering objects with any channels excited is desirable, which would benefit designs of functional devices. In our work of [20], we employ the concept of optimization to address such doubt. We now consider a constant level of σ_{abs} at definite N angular momentum channels excited, then we seek to evaluate the extreme of σ_{scs} . We thus define an energy function L involving SCS and ABS as follows, i.e., $L(a_{-N}, \dots, 0, \dots, a_N) = \sigma_{scs} + \lambda \sigma_{abs}$, where λ is a Lagrange undetermined multiplier. To have the extreme, the energy function needs to simultaneously satisfy $\partial L / \partial |a_i| = 0$ and $\partial L / \partial \theta_i = 0$ for $i = -N \sim N$. Here we express the complex scattering coefficient as $a_i = |a_i|e^{i\theta_i}$ where θ_i is the argument. As a result, we find that under a constant σ_{abs} and with N angular momentum channels involved, there has two extremes of σ_{sc} with one being minimum and another being maximum. We indicate such extreme conditions de-

icted in the solid lines of Figs. 1 (a)-(b). We notice that any scattering systems operated at such conditions would have $|a_i| = constant$ and $\theta_i = \pi$ for $i = -N \sim N$. With these outcomes, we depict the corresponding physical boundary and domain for total normalized SCS defined as $k_0\sigma_{scs}/4$ and normalized ABS defined as $k_0\sigma_{abs}/4$ in Fig. 1 (a), for $N = 0, N = 1, N = 2, N = 3, N = 4$, and $N = 5$ dominant marked by red, orange, yellow, green, pink, and gray colors.

As arbitrary scattering systems with $N = 0, N = 1, N = 2, N = 3, N = 4$, and $N = 5$ dominant, the corresponding maximum normalized SCS, i.e., $k_0\sigma_{scs}/4$, would be 1, 3, 5, 7, 9, and 11, respectively, as clearly shown in Fig. 1 (a). The maximum normalized ABS, i.e., $k_0\sigma_{abs}/4$, for $N = 0, N = 1, N = 2, N = 3, N = 4$, and $N = 5$ dominant, would be 1/4, 3/4, 5/4, 7/4, 9/4, and 11/4, respectively, as clearly shown in Fig. 1 (a). Next, we integrate all results of Fig. 1 (a) into a single normalized cross section diagram in Fig. 1 (b). In addition, by considering $\sigma_{ext} = \sigma_{abs} + \sigma_{scs}$, we also make the contour plot for the normalized EXT defined as $k_0\sigma_{ext}/4$ in Fig. 1 (b). With more N angular momentum channels involved, the domain for SCS, ABS, and EXT would be further extended as well. Moreover, we can see that due to the fact that the domain of larger angular momentum channels surrounds that of lower ones, any scattering systems with more channels involved may behave the same cross sections as by lower channels, exhibiting the degeneracy. In Fig. 1 (b), we observe that along a constant level of normalized EXT, i.e., $k_0\sigma_{ext}/4 = constant$, there enables the gradual decrease of normalized SCS as well as the gradual increase of normalized ABS.

Now, we turn to discuss the corresponding Far-field radiation at the boundary of $N = 1, N = 2, N = 3$, and so on. With a constant normalized EXT and along the N -boundary as in Figs. 1 (a)-(b), the scattering coefficients would satisfy,

$$a_i = -\frac{k_0\sigma_{ext}}{4(2N+1)}, i \in [-N, N]. \quad (1)$$

The corresponding SCS and ABS would be

$$\begin{cases} \sigma_{scs}(N) = \frac{k_0\sigma_{ext}^2}{4(2N+1)} \\ \sigma_{abs}(N) = \sigma_{ext}[1 - \frac{k_0\sigma_{ext}}{4(2N+1)}], \end{cases} \quad (2)$$

and the corresponding differential SCS is

$$\sigma_{scs}^{diff}(\phi) = \frac{k_0\pi\sigma_{ext}^2}{2(2N+1)^2} \frac{1}{2\pi} \sum_{n=-N}^N e^{in\phi} \quad (3)$$

[34], where ϕ is the azimuth of cylindrical coordinate system. Interestingly, we find that the term of $\frac{1}{2\pi} \sum_{n=-N}^N e^{in\phi}$ as $N \rightarrow \infty$ is mathematically equivalent to the discrete Fourier series of the Dirac-delta function

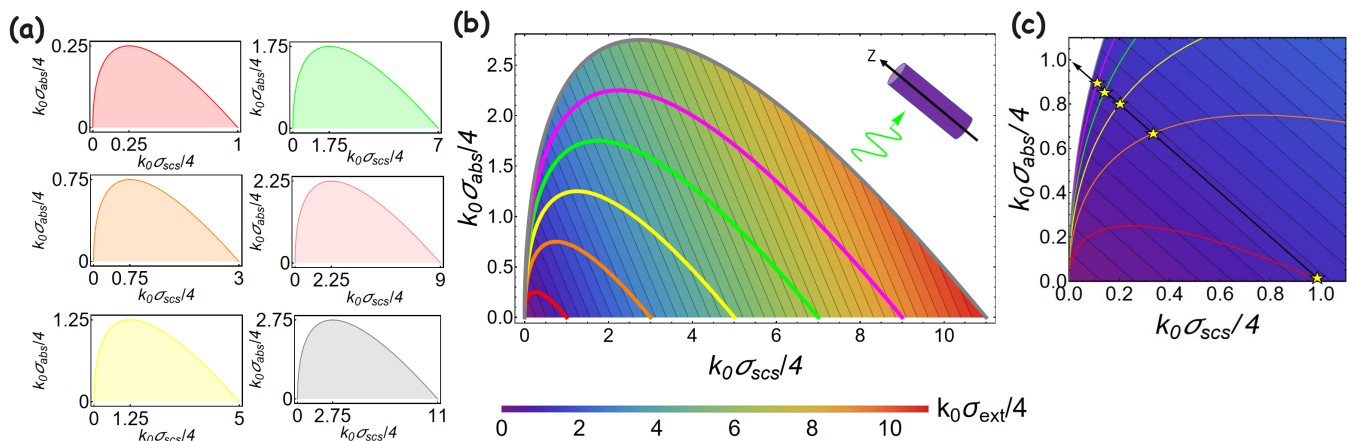


FIG. 1. Physical boundary and domain of normalized SCS ($k_0\sigma_{scs}/4$) and normalized ABS ($k_0\sigma_{abs}/4$) for $N = 0, N = 1, N = 2, N = 3, N = 4, N = 5$ dominant in (a). Integrating these results and considering EXT ($\sigma_{ext} = \sigma_{abs} + \sigma_{scs}$), the contourplot of normalized EXT ($k_0\sigma_{ext}/4$) is provided in (b). Under a constant level of $k_0\sigma_{ext}/4 = 1$, by more N channels involved, the levels of normalized SCS and normalized ABS would be further reduced and increased, respectively, as highlighted by yellow stars in (c).

i.e.,

$$\delta(\phi) = \frac{1}{2\pi} + \frac{1}{\pi} \sum_{n=1}^{\infty} \cos[n\theta] = \frac{1}{2\pi} \sum_{n=-\infty}^{\infty} e^{in\phi} \quad (4)$$

[38]. This result reflects that any scattering systems operated at the N -th boundary would perform a needle Dirac-delta like far-field radiation pattern. We note that such Dirac-delta of radiation, with highly super-directive, had discovered by degenerate resonant channels excited [39].

To demonstrate this result, we choose $k_0\sigma_{ext}/4 = 1$ followed with a black arrow in Fig. 1 (c). Then with N channels involved, the values of ($k_0\sigma_{scs}/4, k_0\sigma_{abs}/4$) for $N = 0, N = 1, N = 2, N = 3, N = 4, N = 5$, would correspond to (1, 0), (1/3, 2/3), (1/5, 4/5), (1/7, 6/7), (1/9, 8/9), (1/11, 10/11), respectively, as marked by yellow stars in Fig. 1 (c). We can see that properly exciting more N channels, there leads to have $\sigma_{scs} \rightarrow 0$ and $\sigma_{abs} \rightarrow \sigma_{ext}$. Then, we depict the far field radiation distribution in Figs. 2 (a)-(b), by considering $N = [5, 10, 100]$, respectively. We can see that except far-field radiation at the forward direction ($\phi = 0$) remains fixed attributed to the fundamental optical theorem, the width of the main lobe gets reduced by increasing N channels. Moreover, the sidelobes get pushed toward the main lobe with respect to N channels, causing an accumulation of ripple around the main lobe, as clearly shown in the insert of Fig. 2 (b). In mathematics, it corresponds to the Gibbs phenomenon, resulting from the discontinuity of a function [38]. We also calculate the null to null bandwidth of the main lobe, i.e., $\sigma_{scs}^{diff}(\phi_{nu}) = 0$, as shown in Fig. 2(c). The result indicates that by more angular momentum channels involved, ϕ_{nu} would get reduced, reducing to perturb the background field.

Now, we design such anomalous subwavelength

nanowires not only with ABS enhanced as well as SCS reduced, but also with the needle Dirac-delta-like far-field radiation. We design non-magnetic, passive, and reciprocal nanowires with multi-layered structures. Then we target $a_n = -1/3$ at $n = [-1, 0, 1]$. As we design such system with $r_1 = 0.142\lambda_0$ (core) and $r_2 = 0.149\lambda_0$ (shell), we numerically find that $\epsilon_1 = -4.7 + 0.058i$ in core and $\epsilon_2 = 51.342 + 23.986i$ in shell can meet the conditions. We provide the multipole analysis of a_n in Fig. 3 (a), consistent with our desired setting. However, there has a small residue at a_2 and a_{-2} , whose magnitude is quite small compared with $a_n = -1/3$ at $n = [-1, 0, 1]$. With COMSOL Multiphysics, we then plot the corresponding far-field radiation pattern of $\sigma_{scs}^{diff}(\phi)$ in Fig. 3 (b), where a small sidelobe is found in the backward direction ($\phi = \pi$). We numerically calculate the null-to-null bandwidth of ϕ_{nu} being 2.042. We also plot the far- and near- field distribution for this two-layered nanowire, where we can observe that a quite large disturbance occurs at the backward and forward directions. In this case, the normalized SCS ($k_0\sigma_{scs}/4$), normalized ABS ($k_0\sigma_{abs}/4$), and normalized EXT ($k_0\sigma_{ext}/4$) are 0.337, 0.729, and 1.066, respectively. We mark that this case is superabsorption, since $k_0\sigma_{abs}/4 = 0.729$ is larger than a single channel limit of $k_0\sigma_{abs}/4 = 0.25$.

Next, we seek to target the condition of $a_n = -1/7$ at $n = [-3, -2, -1, 0, 1, 2, 3]$, belonging to $N = 3$ domain. We find that a four-layered nanowire can fulfil this desired design, with the geometry of $r_1 = 0.151\lambda_0, r_2 = 0.189\lambda_0, r_3 = 0.249\lambda_0,$ and $r_4 = 0.287\lambda_0$ and the material parameters of $\epsilon_1 = 5.149 + 0.561i, \epsilon_2 = 0.113 + 0.011i, \epsilon_3 = 0.302 + 0.037i,$ and $\epsilon_4 = -0.107 + 0.002i$. Then we provide the multipole analysis of a_n in Fig. 3 (d), meeting our requirement of $a_n = -1/7$ from $n = -3$ to $n = 3$, although there still has a small residue from a_{-4} and a_4 . We plot the corresponding far-field radiation pattern in

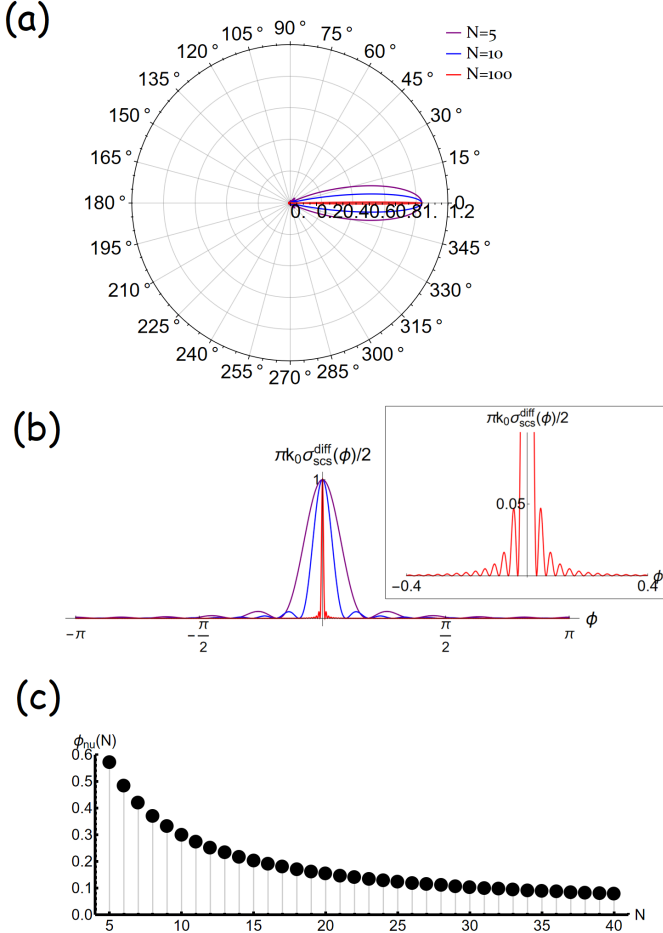


FIG. 2. By considering $N = [5, 10, 100]$ and $k_0\sigma_{ext}/4 = 1$ into Eq.(3), we depict the corresponding far-field radiation in (a) and (b). Here these results are expressed in units of $\pi k_0\sigma_{scs}^{diff}(\phi)/2$. In the insert of (b), we highlight the ripple-like sidelobes, around the main lobe, corresponding to the Gibbs phenomenon. In (c), we calculate the null-to-null bandwidth of the main lobe, i.e., ϕ_{nu} , for $5 \leq N \leq 40$.

Fig. 3 (e), here the radiation is largely reduced except in the forward. Compared with the previous design in Figs. 3 (a)-(c), this nanowire system can exhibit more shaper far-field radiation with $\phi_{nu} = 0.889$, although they all have the same level of EXT. We plot the far- and near- field distributions in Fig. 3 (f). For a comparison, we can observe a more reducing disturbance of the scattering field on the background field. We notice that this scattering system exhibits ABS enhanced and SCS reduced. Here $k_0\sigma_{scs}/4 = 0.143$, $k_0\sigma_{abs}/4 = 0.868$, and $k_0\sigma_{ext}/4 = 1.011$. In the near field distribution, we observe that there has giant electric fields occurred in the shell layers of $r_1 \leq r \leq r_2$ and $r_3 \leq r \leq r_4$, up to $3.5 \times 10^3 [V/m]$, with possible application in strengthening light-matter interaction and nonlinear optics. The extreme field in these shell layers is attributed to the lo-

calized surface plasmon excited.

Now we arrive at two crucial doubts:

- (i) Could there exist an ideal (perfect) needle Dirac-delta scattering radiation, if a_n can be properly excited ?
- (ii) Without following Eq.(1), could any scatterers having near zero of SCS and $\sigma_{abs} \rightarrow \sigma_{ext}$ perform a needle like scattering pattern?

To address (i), we draw support from the Gibbs phenomenon of Fourier theory. Therefore, the formation of the ideal (perfect) needle radiation is excluded, even if one can unlimitedly and properly excite any number of angular momentum channels. Instead, one can have a close affinity of Dirac-Delta like far-field radiation with extreme small ripple-like sidelobes around the main lobe. To address (ii), we resort to the theory of Fourier transform theory and Gibbs phenomenon. Since any dominant a_n following Eq.(1) would have the Dirac-delta-like shape of radiation, any deviation of the Fourier coefficients would deviate to have a needle-like shape. Therefore, any scatterers even with largely reducing SCS and $\sigma_{abs} \rightarrow \sigma_{ext}$ can not guarantee to have a needle-like radiation. Based on our dark superabsorber scheme, we thus calculate a ratio defined as the total radiation from sidelobes over SCS, as follows,

$$\begin{aligned} \epsilon(N) &= \frac{\int_{\phi_{nu}}^{2\pi-\phi_{nu}} \sigma_{scs}^{diff}(\phi) d\phi}{\sigma_{scs}(N)} \\ &= \frac{1}{2\pi(2N+1)} \int_{\phi_{nu}}^{2\pi-\phi_{nu}} \left| \sum_{n=-N}^N e^{in\phi} \right|^2 d\phi. \end{aligned} \quad (5)$$

We provide the numerical results with respect to N in Fig. 4 (a), where we can see that increasing N channels, this ratio would roughly be 0.097. We observe that this result is independence of σ_{ext} . It reveals that the radiation from these sidelobe becomes a residual source for other scatterers without following our scheme. As a result, we expect that these scatterers would radiate not only in the forward direction, but also over other directions. We demonstrate such subwavelength scatterer by using two-layered structure in Figs. 3 (g)-(i) with geometry of $r_1 = 0.333\lambda_0$ and $r_2 = 0.378\lambda_0$ and material parameters of $\epsilon_1 = 1.157 + 0.1i$ and $\epsilon_2 = 0.368 + 0.4i$. In this case, it has $k_0\sigma_{scs}/4 = 0.159$, $k_0\sigma_{abs}/4 = 0.84$, and $k_0\sigma_{ext}/4 = 0.999$ as almost the same values as demonstrated in Figs. 3 (d)-(f). However, as we provide the multipole analysis of a_n , in Fig. 3 (g), we find that this case can not fulfill the Eq.(1). Then we depict the far-field radiation in Fig. 3 (h), where we can observe a small sidelobe occurred at the backward. In Fig. 3 (i), we provide the corresponding far- and near- field distribution, showing the significant disturbance to the background field in the backward and forward directions.

The aim to achieve superdirective scattering radiation has implemented in Yagi-Uda-inspired nanoantennas, Huygens-resonator array, high-order-assisted multipolar resonants to name a few, with benefit of applications in enhanced emission of quantum dots, single

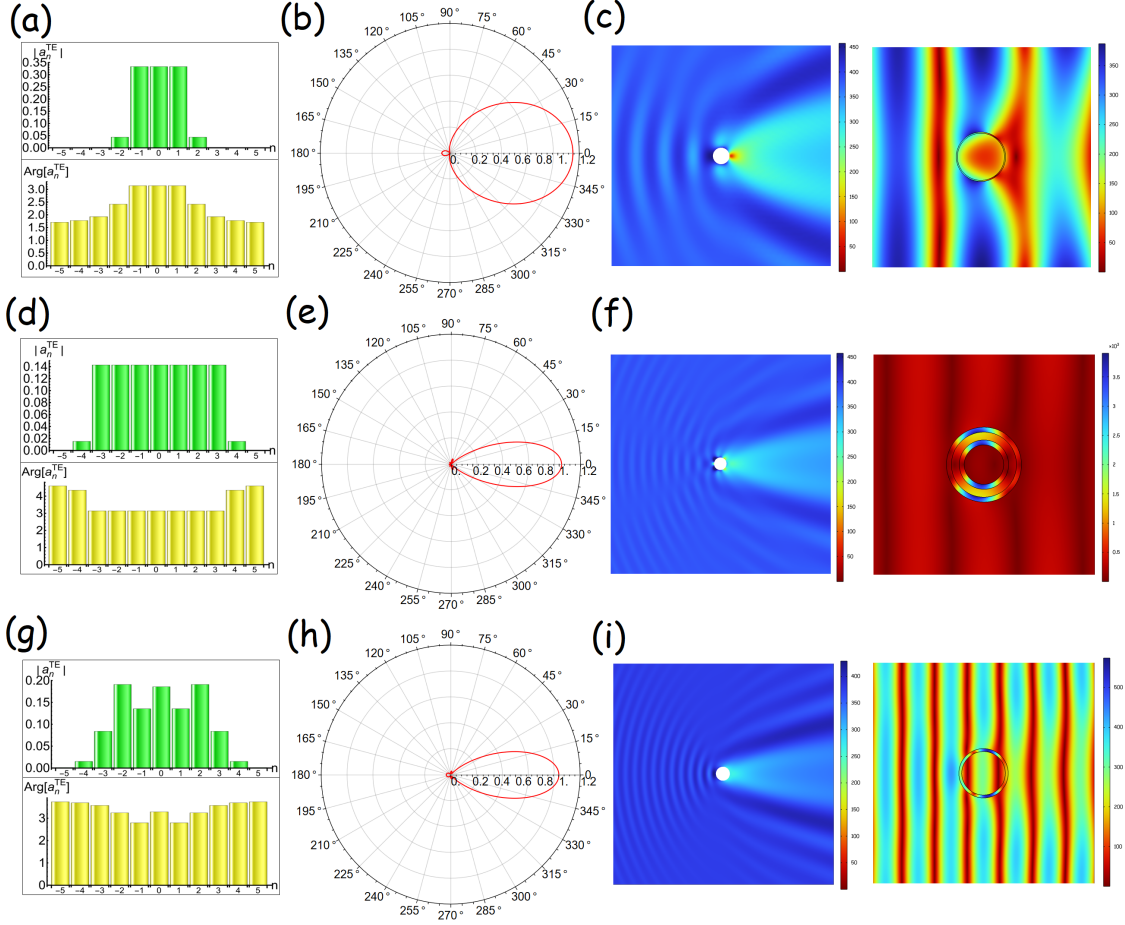


FIG. 3. By designing a two-layered cylindrical nanowire with the geometry of $r_1 = 0.142\lambda_0$ and $r_2 = 0.149\lambda_0$ and the material parameters of $\epsilon_1 = -4.7 + 0.058i$ and $\epsilon_2 = 51.342 + 23.986i$, we provide the multipole analysis of a_n in (a). By exploiting COMSOL Multiphysics, the corresponding far-field radiation, far-field and near-instant field distribution for this design are in shown in (b) and (c). In (d)-(f), there are multipole analysis of a_n , far-field radiation, far-field and near-instant field distribution for another design of a four-layered cylindrical nanowire with the geometry of $r_1 = 0.151\lambda_0$, $r_2 = 0.189\lambda_0$, $r_3 = 0.249\lambda_0$, and $r_4 = 0.287\lambda_0$ as well as the material parameters of $\epsilon_1 = 5.149 + 0.561i$, $\epsilon_2 = 0.113 + 0.011i$, $\epsilon_3 = 0.302 + 0.037i$, and $\epsilon_4 = -0.107 + 0.002i$. Then we design another core-shell cylindrical system by the geometry of $r_1 = 0.333\lambda_0$ and $r_2 = 0.378\lambda_0$ and the material parameters of $\epsilon_1 = 1.157 + 0.1i$ and $\epsilon_2 = 0.368 + 0.4i$. In (g)-(i), we depict the corresponding multipole analysis, far-field radiation, far-field, and near-instant field distribution.

photon emission, wireless power delivery, and Raman scattering [40–54]. Here we demonstrate a whole new scheme to not only have superdirective needle-like radiation, but also have suppressed sidelobes. The resultant outcome is to reduce the disturbance on the background fields, except in the forward. The design of scatterers having maintaining lower-scattering but without sacrificing absorption had been theoretically and experimentally demonstrated, with practical applications on lower-visibility sensors, Fresnel diffractive imaging, and so on [55–61]. As our demonstration in the case of Figs. 3 (g)-(i), targeting the extreme ABS and SCS for such specific designs is insufficient to meet low-observability.

To our summary, we formulate the conditions for any

scattering systems not only with a near same level of ABS as EXT ($\sigma_{abs} \rightarrow \sigma_{ext}$) but also with the Dirac-delta-like far-field radiation, resulting in a reducing distance to the background field except in the forward direction. We refer to the results as dark superabsorbers. Resorting to Gibbs phenomenon of Fourier theory, the perfect single needle-like far-field radiation is excluded, while there are always many ripple sidelobes around the main lobe. We discuss other possible scattering events having enhanced ABS and reduced SCS. We argue that our proposed scheme could offer an optimized reduced perturbation to the background field.

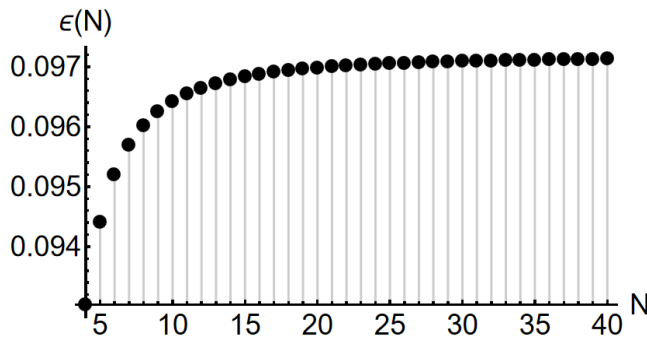


FIG. 4. A radiation ratio of Eq. (5) with respect to N .

ACKNOWLEDGEMENTS

This work was supported by Ministry of Science and Technology, Taiwan (MOST) (107- 2112-M-259-007-MY3, 110-2112-M-259-005- and 111-2112-M-259 -011 -).

-
- [1] Brongersma, Mark L., Yi Cui, and Shanhui Fan. "Light management for photovoltaics using high-index nanostructures." *Nature materials* 13.5 (2014): 451-460.
- [2] Cortés, Emiliano, et al. "Optical metasurfaces for energy conversion." *Chemical Reviews* 122.19 (2022): 15082-15176.
- [3] Otnes, Gaute, and Magnus T. Borgström. "Towards high efficiency nanowire solar cells." *Nano Today* 12 (2017): 31-45.
- [4] Cao, Linyou, et al. "Engineering light absorption in semiconductor nanowire devices." *Nature materials* 8.8 (2009): 643-647.
- [5] Dai, Xing, et al. "GaAs/AlGaAs nanowire photodetector." *Nano letters* 14.5 (2014): 2688-2693.
- [6] Jaque, Daniel, et al. "Nanoparticles for photothermal therapies." *nanoscale* 6.16 (2014): 9494-9530.
- [7] Brigger, Irene, Catherine Dubernet, and Patrick Couvreur. "Nanoparticles in cancer therapy and diagnosis." *Advanced drug delivery reviews* 64 (2012): 24-36.
- [8] Tribelsky, Michael I., et al. "Laser pulse heating of spherical metal particles." *Physical Review X* 1.2 (2011): 021024.
- [9] Ladutenko, Konstantin, et al. "Superabsorption of light by nanoparticles." *Nanoscale* 7.45 (2015): 18897-18901.
- [10] Mirzaei, Ali, et al. "Superabsorption of light by multi-layer nanowires." *Nanoscale* 7.42 (2015): 17658-17663.
- [11] Bai, Ping, Ying Wu, and Yun Lai. "Multi-channel coherent perfect absorbers." *Europhysics Letters* 114.2 (2016): 28003.
- [12] Estakhri, Nasim Mohammadi, and Andrea Alù. "Minimum-scattering superabsorbers." *Physical Review B* 89.12 (2014): 121416.
- [13] Ruan, Zhichao, and Shanhui Fan. "Superscattering of light from subwavelength nanostructures." *Physical review letters* 105.1 (2010): 013901.
- [14] Ruan, Zhichao, and Shanhui Fan. "Design of subwavelength superscattering nanospheres." *Applied Physics Letters* 98.4 (2011): 043101.
- [15] Qian, Chao, et al. "Experimental observation of superscattering." *Physical review letters* 122.6 (2019): 063901.
- [16] Jia, Yiming, et al. "Theory of half-space light absorption enhancement for leaky mode resonant nanowires." *Nano Letters* 15.8 (2015): 5513-5518.
- [17] Canós Valero, Adrià, et al. "Superscattering emerging from the physics of bound states in the continuum." *Nature Communications* 14.1 (2023): 4689.
- [18] Miroschnichenko, Andrey E., and Michael I. Tribelsky. "Ultimate absorption in light scattering by a finite obstacle." *Physical review letters* 120.3 (2018): 033902.
- [19] Lee, Jeng Yi, and Ray-Kuang Lee. "Phase diagram for passive electromagnetic scatterers." *Optics Express* 24.6 (2016): 6480-6489.
- [20] Lee, Jeng Yi, Yi-Huan Chen, and Pai-Yen Chen. "Degeneracy of light scattering and absorption by a single nanowire." *Scientific Reports* 11.1 (2021): 18657.
- [21] J. D. Jackson, *Classical Electrodynamics* (John Wiley & Sons, New York, 2001), Chap. X.
- [22] Alu, Andrea, and Nader Engheta. "How does zero forward-scattering in magnetodielectric nanoparticles comply with the optical theorem?." *Journal of Nanophotonics* 4.1 (2010): 041590.
- [23] Kerker, Milton, D-S. Wang, and C. L. Giles. "Electromagnetic scattering by magnetic spheres." *JOSA* 73.6 (1983): 765-767.
- [24] Lee, Jeng Yi, Andrey E. Miroschnichenko, and Ray-Kuang Lee. "Reexamination of Kerker's conditions by means of the phase diagram." *Physical Review A* 96.4 (2017): 043846.
- [25] Qin, Feifei, et al. "Transverse Kerker effect for dipole sources." *Physical Review Letters* 128.19 (2022): 193901.
- [26] Olmos-Trigo, Jorge, et al. "Kerker conditions upon lossless, absorption, and optical gain regimes." *Physical Review Letters* 125.7 (2020): 073205.
- [27] Olmos-Trigo, Jorge, et al. "Optimal backward light scattering by dipolar particles." *Physical Review Research* 2.1 (2020): 013225.
- [28] Liu, Wei, and Yuri S. Kivshar. "Generalized Kerker effects in nanophotonics and meta-optics." *Optics express* 26.10 (2018): 13085-13105.
- [29] Shamkhi, Hadi K., et al. "Transverse scattering and generalized kerker effects in all-dielectric mie-resonant metaoptics." *Physical review letters* 122.19 (2019): 193905.
- [30] Lee, Jeng Yi, Andrey E. Miroschnichenko, and Ray-Kuang Lee. "Simultaneously nearly zero forward and nearly zero backward scattering objects." *Optics express* 26.23 (2018): 30393-30399.

- [31] Souнас, Dimitrios L., and Andrea Alù. "Extinction symmetry for reciprocal objects and its implications on cloaking and scattering manipulation." *Optics letters* 39.13 (2014): 4053-4056.
- [32] Cheng, Lin, et al. "Superscattering, superabsorption, and nonreciprocity in nonlinear antennas." *ACS Photonics* 8.2 (2021): 585-591.
- [33] Hulst, Hendrik Christoffel, and Hendrik C. van de Hulst. *Light scattering by small particles*. Courier Corporation, 1981.
- [34] Bohren, Craig F., and Donald R. Huffman. *Absorption and scattering of light by small particles*. John Wiley & Sons, 2008.
- [35] Baranov, Denis G., et al. "Coherent perfect absorbers: linear control of light with light." *Nature Reviews Materials* 2.12 (2017): 1-14.
- [36] Noh, Heeso, et al. "Perfect coupling of light to surface plasmons by coherent absorption." *Physical review letters* 108.18 (2012): 186805.
- [37] Chong, Y. D., et al. "Coherent perfect absorbers: time-reversed lasers." *Physical review letters* 105.5 (2010): 053901.
- [38] Gbur, Gregory J. *Mathematical methods for optical physics and engineering*. Cambridge University Press, 2011.
- [39] Arslanagić, Samel, and Richard W. Ziolkowski. "Highly subwavelength, superdirective cylindrical nanoantenna." *Physical Review Letters* 120.23 (2018): 237401.
- [40] Maksymov, Ivan S., et al. "Optical yagi-uda nanoantennas." *Nanophotonics* 1.1 (2012): 65-81.
- [41] Ho, Jinfa, et al. "Highly directive hybrid metal-dielectric Yagi-Uda nanoantennas." *ACS nano* 12.8 (2018): 8616-8624.
- [42] Dregely, Daniel, et al. "3D optical Yagi-Uda nanoantenna array." *Nature communications* 2.1 (2011): 267.
- [43] Kullock, René, et al. "Electrically-driven Yagi-Uda antennas for light." *Nature communications* 11.1 (2020): 115.
- [44] Ziolkowski, Richard W. "Using Huygens multipole arrays to realize unidirectional needle-like radiation." *Physical Review X* 7.3 (2017): 031017.
- [45] Lin, Wei, Richard W. Ziolkowski, and Jianquan Huang. "Electrically small, low-profile, highly efficient, Huygens dipole rectennas for wirelessly powering Internet-of-Things devices." *IEEE Transactions on Antennas and Propagation* 67.6 (2019): 3670-3679.
- [46] Krasnok, Alexander E., et al. "Superdirective dielectric nanoantennas." *Nanoscale* 6.13 (2014): 7354-7361.
- [47] Alù, Andrea, and Nader Engheta. "Wireless at the nanoscale: optical interconnects using matched nanoantennas." *Physical review letters* 104.21 (2010): 213902.
- [48] Yesilyurt, Ayse Tugca Mina, et al. "Unidirectional Meta-Emitters Based on the Kerker Condition Assembled by DNA Origami." *ACS nano* 17.19 (2023): 19189-19196.
- [49] Damasceno, Gabriel HB, et al. "Magnetoplasmonic nanoantennas for on-chip reconfigurable optical wireless communications." *ACS Applied Materials & Interfaces* 15.6 (2023): 8617-8623.
- [50] Kosako, Terukazu, Yutaka Kadoya, and Holger F. Hofmann. "Directional control of light by a nano-optical Yagi-Uda antenna." *Nature Photonics* 4.5 (2010): 312-315.
- [51] Zhang, Yinan, et al. "Ultra-broadband directional scattering by colloiddally lithographed high-index Mie resonant oligomers and their energy-harvesting applications." *ACS applied materials & interfaces* 10.19 (2018): 16776-16782.
- [52] Yang, Yuanqing, et al. "Multimode directionality in all-dielectric metasurfaces." *Physical Review B* 95.16 (2017): 165426.
- [53] Fu, Yuan Hsing, et al. "Directional visible light scattering by silicon nanoparticles." *Nature communications* 4.1 (2013): 1527.
- [54] Liu, Wei, et al. "Broadband unidirectional scattering by magneto-electric core-shell nanoparticles." *ACS nano* 6.6 (2012): 5489-5497.
- [55] Soric, Jason C., et al. "Dual-polarized reduction of dipole antenna blockage using mantle cloaks." *IEEE Transactions on Antennas and Propagation* 63.11 (2015): 4827-4834.
- [56] Monticone, Francesco, Christos Argyropoulos, and Andrea Alu. "Optical antennas: controlling electromagnetic scattering, radiation, and emission at the nanoscale." *IEEE Antennas and Propagation Magazine* 59.6 (2017): 43-61.
- [57] Soric, Jason C., et al. "Controlling scattering and absorption with metamaterial covers." *IEEE Transactions on Antennas and Propagation* 62.8 (2014): 4220-4229.
- [58] Butun, Serkan, and Koray Aydin. "Structurally tunable resonant absorption bands in ultrathin broadband plasmonic absorbers." *Optics express* 22.16 (2014): 19457-19468.
- [59] Raad, Shiva Hayati, Mehdi Afshari-Bavil, and Dong Liu. "Efficient and high-quality absorption enhancement using epsilon-near-zero cylindrical nano-shells constructed by graphene." *Scientific Reports* 14.1 (2024): 6742.
- [60] Nishijima, Yoshiaki, et al. "Absorption and scattering in perfect thermal radiation absorber-emitter metasurfaces." *Optics Express* 30.3 (2022): 4058-4070.
- [61] Alù, Andrea, and Nader Engheta. "Cloaking a sensor." *Physical review letters* 102.23 (2009): 233901.